General, Spontaneous Ion Replacement Reaction for the Synthesis of Micro- and Nanostructured Metal Oxides

Chenglin Yan and Dongfeng Xue*

State Key Laboratory of Fine Chemicals, Department of Materials Science and Chemical Engineering, School of Chemical Engineering, Dalian University of Technology, 158 Zhongshan Road, Dalian 116012, People's Republic of China

Received: November 4, 2005; In Final Form: December 12, 2005

A novel spontaneous ion replacement route based on the solubility difference as the driving force to synthesize a number of metal oxides has been established. We present a comprehensive study on the ion replacement reaction for chemical synthesis of micro- and nanostructured Mn_2O_3, ZnO, CuO, CdO, Al_2O_3, and CaO samples. This novel approach described herein is derived from the solubility difference between two carbonate salts, in which a metal cation can be driven from one liquid phase into another solid phase in the solution system. The resulting metal carbonate salts are initially formed and subsequently calcined to form highly crystallined metal oxides. The variation of pH values, reaction temperature, and reagent shapes can vary the solubility of these two carbonate salts, which thus changes the final morphology of metal oxides. The present work makes a progress to simply and mildly synthesize metal oxides with various morphologies, due to the fact that materials with a desired morphology are a key engineering step toward their shape-dependent chemical and physical properties.

1. Introduction

In recent years, intensive research attention has been increasingly drawn in an effort to synthesize micro- and nanomaterials for their fundamental size, morphology-dependent properties, and many important technological applications,[1−10] which are derived from their low dimensionality combined with the quantum confinement effect.[11,12] Metal oxides, in particular, represent one of the most diverse classes of materials, with important structure-related properties including superconductivity, solar cells, catalysis, magnetism, and gas sensors.[13−20] The challenge of developing new synthetic methods for a variety of metal oxides is the ability to demonstrate our development of a generalized synthetic method. Recently, many effective approaches have been developed to fabricate metal oxide materials, such as the chemical vapor transport process,[15a] electrodeposition,[21] template-directed growth,[22] sol−gel processes,[23] and coprecipitation synthetic method.[24] In the current work, the spontaneous ion replacement reaction as a novel and effective method is carried out to demonstrate its strong ability of the synthesis of micro- and nanostructured metal oxides.

As one of the widely used routes, the direct precipitation method allows us to give a minute control over the shape and size, due to the rapid precipitation under high supersaturation in a short time. The use of a simple spontaneous ion replacement reaction may be an effective method offering a better control over the morphology and size in contrast to the direct precipitation reaction. Here we demonstrate that the scope of ion replacement method could be extended to process a number of metal oxides. This novel synthetic approach also allows further reducing the growth temperature to room temperature, leading to the development of an effective, low-cost fabrication process and good potential for scale up.

* To whom correspondence should be addressed. E-mail: dfxue@chem.dlut.edu.cn.

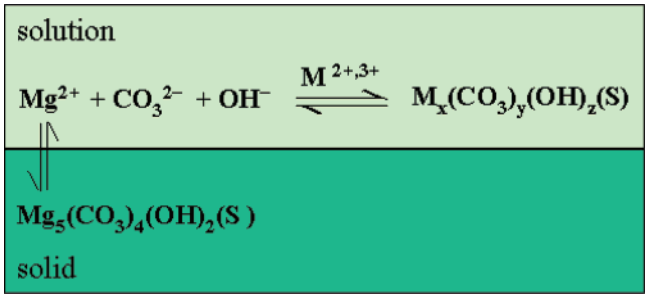

Figure 1. A schematic diagram of the spontaneous ion replacement process in an aqueous solution. M = Mn, Zn, Cu, Cd, Ca, or Al; *x*, *y*, *z* = 0, 1, 2, 3, 4, or 5.

The novel approach described herein is derived from the solubility difference between two carbonate salts, in which metal cations can be driven from one liquid phase into one solid phase in the solution system. The whole reaction process of the ion replacement reaction is schematically displayed in Figure 1. The resulting metal carbonate salts are initially formed and subsequently calcined to form highly crystallined metal oxides. In a typical synthesis, $M_x(CO_3)_y(OH)_z$ (*x*, *y*, *z* = 0, 1, 2, 3, 4, or 5) particles are obtained by replacement of Mg^{2+} with $M^{2+,3+}$ through the following reaction

$$M^{2+,3+} + Mg_5(CO_3)_4(OH)_2(s) \leftrightarrow M_x(CO_3)_y(OH)_z(s) + Mg^{2+} \quad (1)$$

Since the K_{sp} coefficient (the solubility product constant K_{sp} is the product of the molar concentrations of the ions formed by the dissociation of a slightly soluble salt each raised to the power of the coefficient in the dissociation equation) for $Mg_5(CO_3)_4(OH)_2$ is higher than that of $M_x(CO_3)_y(OH)_z$ at the same reaction conditions, which implies a tendency for the reaction to progress toward the target samples, the chemical

10.1021/jp056373+ CCC: $33.50
Published on Web 01/10/2006

equilibrium in eq 1 moves to the right side. In this work, we present a novel study on the ion replacement reaction for the synthesis of micro- and nanostructured Mn_2O_3, ZnO, CuO, CdO, Al_2O_3, and CaO.

2. Experimental Section

Micro- and nanostructured Mn_2O_3, ZnO, CuO, CdO, Al_2O_3, and CaO were obtained by pyrolysis of their corresponding precursors at designed temperatures, these precursors were synthesized by the ion replacement reaction of $M^{2+,3+}$ (where M = Mn, Zn, Cu, Cd, Al, or Ca) and $Mg_5(CO_3)_4(OH)_2$ in the solution system. All chemical reagents used in this experiment were of analytical grade. The detailed synthesis procedures were described as follows. To prepare both Mn_2O_3 and CdO, 0.015 mol $MnSO_4$ or $CdSO_4$ was dissolved in deionized water in a 50-mL beaker, 0.002 mol $Mg_5(CO_3)_4(OH)_2$ powder was then added, and a suspension solution was obtained. This beaker was then filled with water up to 80% of the total volume. The suspension solution was rapidly adjusted to a designated pH value using HCl solution (1 M) or $NH_3{\cdot}H_2O$ (25 wt %) solution. The reaction mixture solution was left at room temperature around 24 h. To prepare ZnO, CaO, and Al_2O_3 (which are not available at room temperature), 0.03 mol $Zn(CH_3COOH)_2$, $CaCl_2$, or $Al_2(SO_4)_3$ was dissolved in deionized water and followed by the addition of 0.002 mol $Mg_5(CO_3)_4(OH)_2$ powders. HCl solution (1 M) or $NH_3{\cdot}H_2O$ (25 wt %) solution was added into the vigorously stirred mixture with the aim to adjust the pH value to the desirable value. The mixture was transferred into a Teflon-lined autoclave of 40 mL capacity. The autoclave was then filled with water up to 80% of the total volume and sealed into an electric oven and maintained at 95−180 °C for 24 h. All final samples were collected, filtered off, washed with deionized water and absolute ethanol several times (to remove any possible ionic remnants), respectively. Finally, these samples were dried in air at 60 °C for 4 h. Mn_2O_3, ZnO, CuO, CdO, Al_2O_3, and CaO were obtained by pyrolysis of their corresponding precursors. Nanostructured CuO was obtained by pyrolysis of its precursor, which was synthesized by the ion replacement reaction between Cu^{2+} and $Mg_5(CO_3)_4(OH)_2$ similar to the synthesized method for the ZnO except for the introduction of 0.4 g of poly(ethylene glycol) (PEG) into the reaction solution. The as-prepared sample was characterized by X-ray diffraction (XRD) on a Rigaku-DMax 2400 diffractometer equipped with the graphite monochromatized Cu Kα radiation. Scanning electron microscopy (SEM) images were taken with a JEOL-5600 LV scanning electron microscope, using an accelerating voltage of 20 kV. Infrared spectra of the $MnCO_3$ samples were measured by a Nicolet Fourier transform infrared (FTIR) spectrometer.

3. Results and Discussion

The crystal structure is determined by XRD measurements. Figure 2a shows the typical diffraction pattern of $MnCO_3$ by the spontaneous ion replacement of $Mg_5(CO_3)_4(OH)_2$ with Mn^{2+} at room temperature, which can be readily indexed as the hexagonal $MnCO_3$ structure with lattice constants $a = 4.79$ and $c = 15.69$ Å (JCPDS, 44-1472). No peaks of impurities such as $Mg_5(CO_3)_4(OH)_2$, etc., can be detected, indicating a high purity of $MnCO_3$ cubes. The pyrolysis of $MnCO_3$ cubes results in Mn_2O_3 cubes; the diffraction pattern of the obtained Mn_2O_3 sample is shown in Figure 2b. All strong peaks may be indexed as the cubic phase α-Mn_2O_3 with the calculated cell parameter $a = 9.405$ Å, which is in a good agreement with the value in the literature (9.405 Å, JCPDS 71-0636). The compositional purity of ZnO, CuO, CdO, CaO, and Al_2O_3 is also confirmed by XRD measurements, which is shown in Figure 3. All reflections in parts a−e of Figure 3 can be readily indexed to the hexagonal phase ZnO (JCPDS 79-0206), monoclinic phase CuO (JCPDS 05-0661), cubic phase CdO (JCPDS 75-1529), cubic phase CaO (JCPDS 48-1467), and hexagonal phase Al_2O_3 (JCPDS 10-0173). These results are in a good agreement with those reports in the literature, which have proven our successful synthesis of these metal oxides.

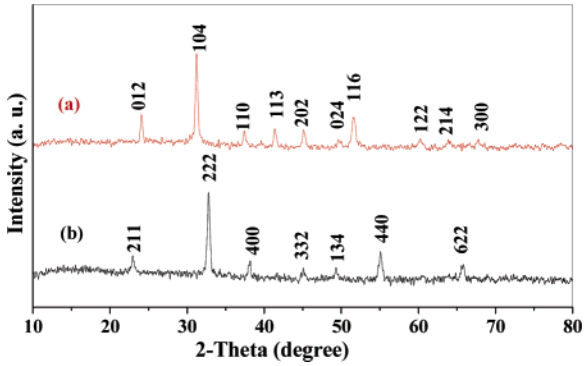

Figure 2. XRD patterns of $MnCO_3$ and Mn_2O_3. (a) $MnCO_3$ cubes obtained by the spontaneous ion replacement reaction at room temperature. (b) Mn_2O_3 cubes obtained by calcination of $MnCO_3$ cubes at 600 °C.

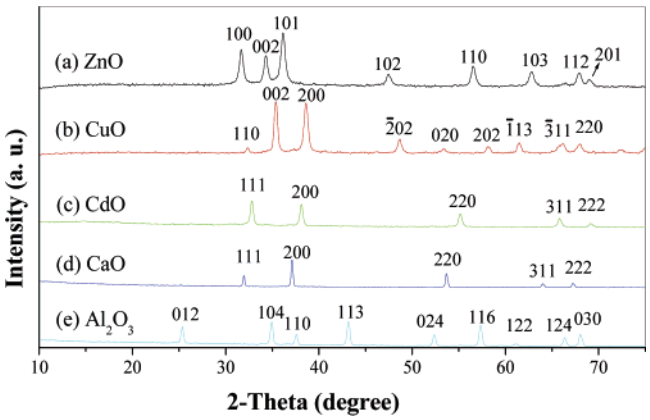

Figure 3. XRD patterns of metal oxides obtained by the spontaneous ion replacement reaction. (a) Hexagonal phase ZnO (JCPDS 79-0206). (b) Monoclinic-phase CuO (JCPDS 05-0661). (c) Cubic-phase CdO (JCPDS 75-1529). (d) Cubic-phase CaO (JCPDS 48-1467). (e) Hexagonal-phase Al_2O_3 (JCPDS 10-0173).

Manganese oxides have drawn considerable attention because of their distinctive properties and now are widely used as electrode materials, catalysts, and soft magnetic materials.[17,18] In the present work, monodispersed α-Mn_2O_3 cubes have been successfully obtained by the pyrolysis of $MnCO_3$ cube precursor, which is synthesized by the simply spontaneous ion replacement of Mg^{2+} with Mn^{2+} between $MnSO_4$ and $Mg_5(CO_3)_4(OH)_2$ in the solution at room temperature. SEM images (parts a−c of Figure 4) of α-Mn_2O_3 cubes show that they are perfect in shape and have the high yielding with a good quality; furthermore, the morphology of α-Mn_2O_3 is very similar to that of its $MnCO_3$ precursor (Supporting Information, Figure SI-1). When 0.2 g of PEG is added to the initial reaction mixture for the synthesis of $MnCO_3$ cubes (keeping all other synthetic conditions unchanged), the obtained cubic $MnCO_3$ are interestingly encapsulated by a cube-shaped transparent layer, as shown in Figure 4d. IR spectra show that no PEG can be found in these transparent $MnCO_3$ cubes (Figure SI-2).

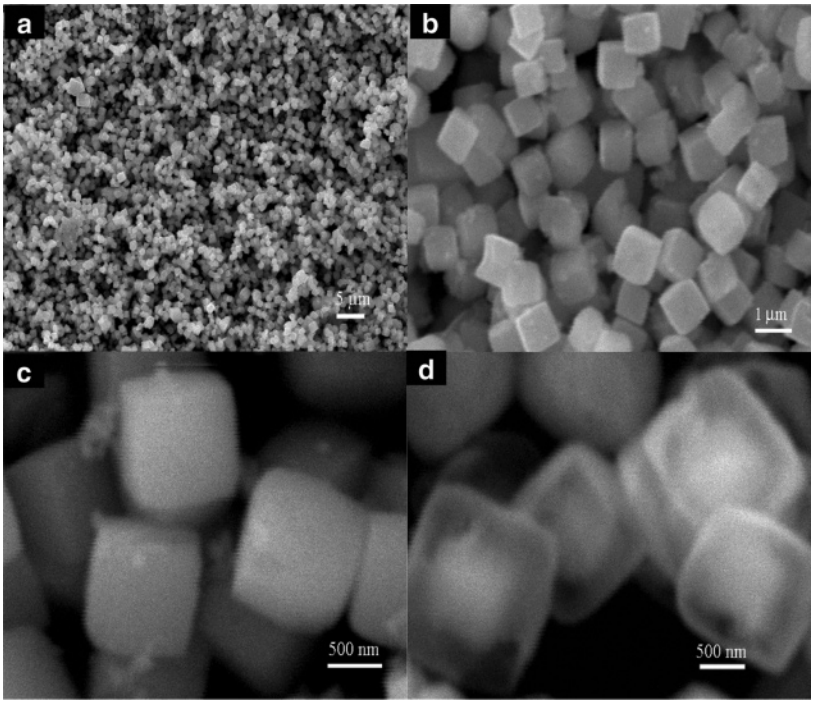

Figure 4. SEM images of Mn_2O_3 and $MnCO_3$ cubes. (a−c) SEM images of monodispersed and well-shaped Mn_2O_3 cubes obtained by calcination of $MnCO_3$ at 600 °C. (d) $MnCO_3$ cubes synthesized by the ion replacement reaction in the presence of PEG.

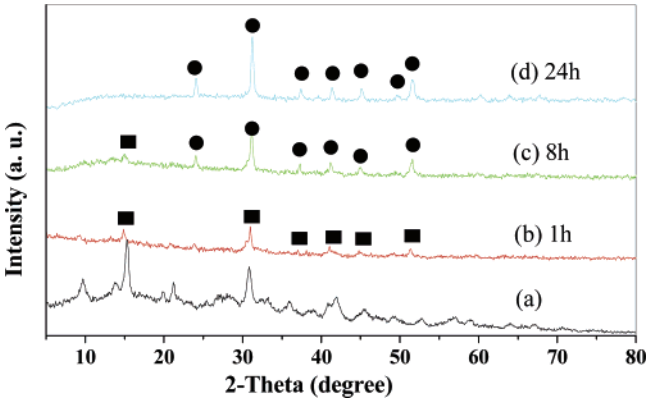

Figure 5. Evolution of the XRD patterns from pure-phase $Mg_5(CO_3)_4(OH)_2$ to $MnCO_3$ by the spontaneous ion replacement reaction with different reaction time at room temperature. (a) Pure phase of $Mg_5(CO_3)_4(OH)_2$ (denoted with solid squares). (b and c) Mixed phase of $Mg_5(CO_3)_4(OH)_2$ and $MnCO_3$. (d) Pure phase of $MnCO_3$ (denoted with solid circles).

In the above experiments, it is assumed that the spontaneous ion replacement reaction is chemically driven by the solubility difference between $Mg_5(CO_3)_4(OH)_2$ and $MnCO_3$ in the aqueous solution, since the K_{sp} coefficient for $Mg_5(CO_3)_4(OH)_2$ is higher than that of $MnCO_3$ at the same conditions. Figure 5 shows the evolution of XRD patterns from a pure-phase $Mg_5(CO_3)_4(OH)_2$ to $MnCO_3$ by the spontaneous ion replacement reaction with different reaction time at room temperature. After 1-h reaction, the intensity of $Mg_5(CO_3)_4(OH)_2$ peaks becomes much weaker, and some peaks disappear gradually. When the reaction time is lengthened up to 8 h, $Mg_5(CO_3)_4(OH)_2$ gradually transforms into $MnCO_3$, and the characteristic peaks of $MnCO_3$ appear. The XRD pattern of compounds obtained after 24 h shows that $Mg_5(CO_3)_4(OH)_2$ phase disappears completely, and only a pure-phase $MnCO_3$ exists. This indicates that the $Mg_5(CO_3)_4(OH)_2$ phase is consumed and that only a pure-phase $MnCO_3$ is produced. On the basis of the experiment results, it was believed that the conversion process from $Mg_5(CO_3)_4(OH)_2$ to $MnCO_3$ is very slow. The solubility difference between $Mg_5(CO_3)_4(OH)_2$ and $MnCO_3$ can be regarded as the main driving force to produce the target compound. The reaction rate is strongly dependent on the degree of solubility difference between two basic carbonate salts. Normally, the bigger the solubility difference, the faster the reaction rate.

Micro- and nanostructured ZnO, CuO, and CdO are obtained by calcination of their corresponding precursors, which are synthesized by the ion replacement reaction of M^{2+} (M = Zn, Cu, or Cd) and $Mg_5(CO_3)_4(OH)_2$ in the solution. The micro- and nanostructure characteristics of the as-prepared samples are examined by SEM measurements. It can be seen from Figure 6a that the obtained polyhedra ZnO samples contain a mixture of well-faced ZnO cubes, hexahedron, and truncated cubes. A higher-magnification SEM image of one polyhedron in Figure 6b indicates that its surfaces are extremely smooth. In Figure 6c, the panoramic morphology of CuO sample shows that the sample consists of nanometer ribbons grown on the surface in a random pattern in high quantity. As can be seen from the magnified image in Figure 6d, the nanoribbons pointing toward the center of dandelion sphere are self-assembled into microscale hierarchical structures. The spherical CdO samples with a rough surface and a diameter of around 5 μm (parts e and f of Figure 5) are obtained by calcination of CdO precursor at 600 °C, which is also produced via the ion replacement reaction between $CdSO_4$ and $Mg_5(CO_3)_4(OH)_2$.

The ion replacement reaction has also been shown to yield the high quality of CaO, Al_2O_3, and CdO samples. SEM image in Figure 7a shows that the synthesized samples are composed of CaO multipod structures, which look like flowers (in which each pod radially grows from one center). A high-magnified SEM image (Figure 7b) shows that the individual CaO rod exhibits a hexagonal prismlike morphology with a hexagonal pyramidlike sharp tip. Spherical Al_2O_3 particles (parts c and d of Figure 7) with smooth surfaces can be obtained by pyrolysis of Al_2O_3 precursor at 1150 °C, which can be synthesized via the ion replacement reaction of Al^{3+} and $Mg_5(CO_3)_4(OH)_2$ at 110 °C. The obtained spherical Al_2O_3 samples are a little

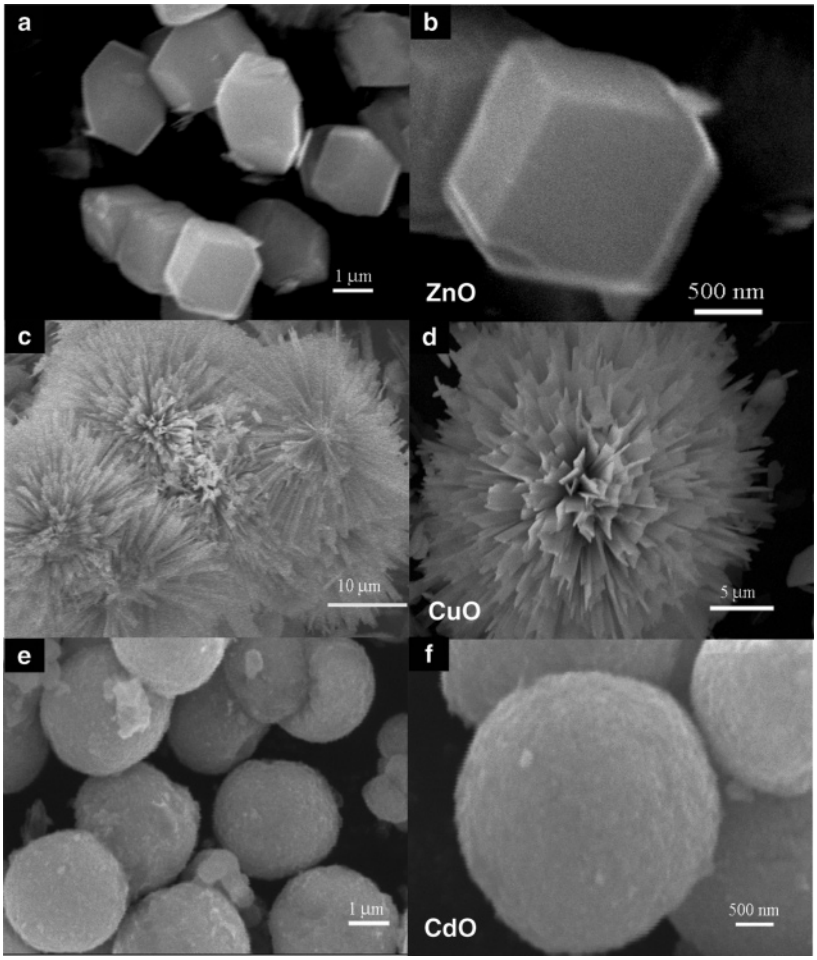

Figure 6. SEM images of ZnO, CuO and CdO oxides. (a and b) Polyhedral ZnO particles containing of hexahedron, cubes, and truncated cubes. (c and d) Self-assembled CuO nanoribbons with a hierarchical structure. (e and f) Spherical CdO particles with rough surfaces.

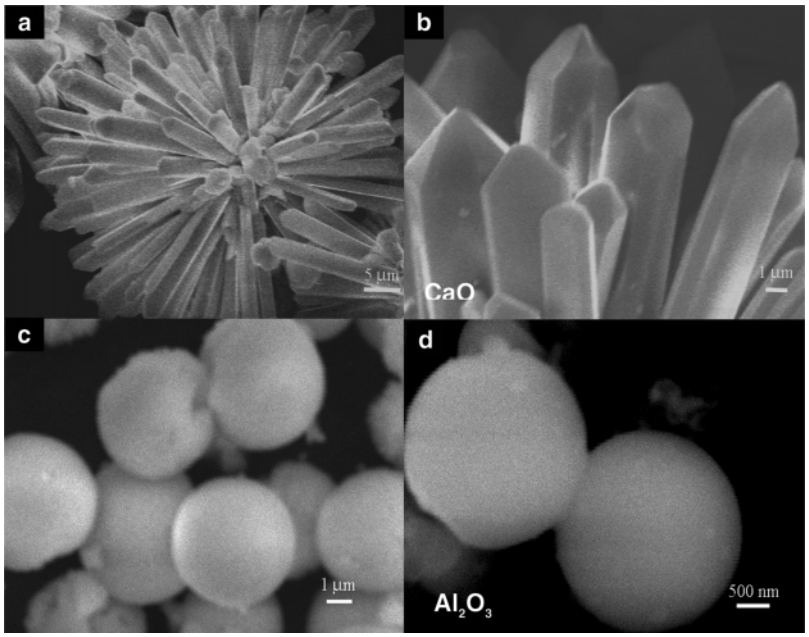

Figure 7. SEM images of CaO and Al_2O_3. (a and b) Self-assembled rodlike CaO particles. (c and d) Spherical Al_2O_3 with smooth surfaces.

different from that of the synthesized spherical CdO samples (Figure 6f) with rough surfaces. The above experimental results indicate that the ion replacement method as a novel and simple method shows a strong ability to the synthesis of many metal oxides with well-defined morphologies.

As pH value of the initial reaction solution affect the solubility, the effect of pH value on the morphology of $MnCO_3$ is investigated by SEM measurements. The morphology of $MnCO_3$ samples can be changed by varying pH values. The monodispersed $MnCO_3$ cubes in large quantities can be obtained

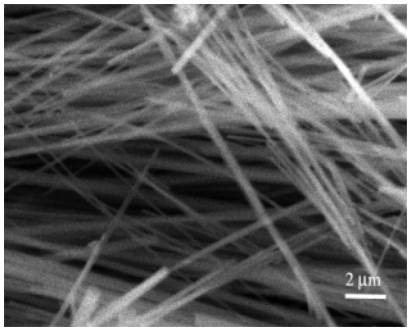

Figure 8. SEM image of ZnO nanowires obtained by the spontaneous ion replacement reaction between Zn^{2+} and nestlike $Mg_5(CO_3)_4(OH)_2$.

at pH = 6 (Figure SI-1). When the pH value is up to 7, the obtained $MnCO_3$ samples contain a mixture of cubic and ellipsoidal $MnCO_3$ (Figure SI-3a). As pH value is further increased to 8, spherical $MnCO_3$ with smooth surfaces can be obtained (Figure SI-3b). Generally speaking, the growth process of crystals can be separated into two steps: an initial nucleation stage and a subsequent crystal growth process. In the subsequent step, the crystal growth stage is a kinetically and thermodynamically controlled process that can yield complicated morphologies. It should be noted that at increasing pH values the solubility of $Mg_5(CO_3)_4(OH)_2$ decreases, while a little variation of solubility is happened to $MnCO_3$ according to the common ion effect.[25] That is, the pH value has a greater influence on the solubility for $Mg_5(CO_3)_4(OH)_2$ than that of $MnCO_3$. Therefore, an increase of pH value causes a decrease of the ion replacement reaction rate. The pH variation of the initial solution results in the change of solubility difference, which further leads to different nucleation and growth rates, and then the $MnCO_3$ morphology changes. These observations indicate that a relatively lower pH value is favorable for the growth of well-shaped $MnCO_3$ cubes.

Besides pH value, temperature is found to play an important role in determining the morphology of samples. A variation of temperature causes a change of solubility difference, which further leads to the variation of the ion replacement reaction rate. The dependence of morphology on temperature is examined by SEM measurements. The ellipselike $MnCO_3$ particles can be obtained at lower reaction temperature of 110 °C and pH = 8 (Figure SI-3c). However, when the temperature is increased up to 180 °C, the ellipselike $MnCO_3$ particles are changed into the rectanglelike morphology (Figure SI-3d). Temperature affects the solubility of reagents, which further influences the crystal nucleation and growth processes. Therefore, the final morphology of samples is changed with the reaction temperature.

In particular, further experiments show that the morphology of our metal oxides can be tuned by changing the shape of $Mg_5(CO_3)_4(OH)_2$ reagent. Figure 8 shows an SEM image of ZnO nanowires prepared by replacing the commercially supplied $Mg_5(CO_3)_4(OH)_2$ (Figure SI-4a) with the nestlike $Mg_5(CO_3)_4(OH)_2$ (Figure SI-4b). In contrast to the well-faced polyhedral ZnO samples synthesized by the ion replacement reaction (between the commercially supplied $Mg_5(CO_3)_4(OH)_2$ and Zn^{2+}) shown in Figure 5a, it can be concluded that $Mg_5(CO_3)_4(OH)_2$ with different micro- and nanostructures leads to the morphology change of ZnO samples. Generally speaking, any crystal with a smaller size always possesses a higher solubility, which thus affects the ion replacement reaction rate, and further exerts a strong influence on the nucleation, subsequent growth and final morphology of samples. In contrast to the commercially supplied $Mg_5(CO_3)_4(OH)_2$ with a larger size, the nestlike $Mg_5(CO_3)_4(OH)_2$ composed of individual nanosheets with a smaller size can have a higher solubility than the commercial $Mg_5(CO_3)_4(OH)_2$. By replacement of the commercially supplied $Mg_5(CO_3)_4(OH)_2$ with the nestlike $Mg_5(CO_3)_4(OH)_2$ as the current reagent, the chemical equilibrium in eq 1 moves much faster to the right side. Furthermore, the unique surface structure of the nestlike $Mg_5(CO_3)_4(OH)_2$ may be used as an active and support site for the perfect growth of ZnO nanowires, due to the fact that it can produce high-quality nanowires with a good and uniform shape (as shown in Figure 8). Therefore, a judicious choice of the shape of $Mg_5(CO_3)_4(OH)_2$ reaction reagent allows us to fabricate various morphologies of our target samples. $Mg_5(CO_3)_4(OH)_2$ reagent with different structure characteristics leads to different nucleation and growth mechanisms during such an ion replacement reaction.

4. Conclusion

The current work demonstrates a room temperature and hydrothermal preparation of metal oxides using a novel spontaneous ion replacement methodology. We present the study on the ion replacement reaction for the controlled synthesis of micro- and nanostructured Mn_2O_3, ZnO, CuO, CdO, Al_2O_3, and CaO samples by starting from their different solubility behaviors of two carbonate salts. From the current experiments, the applied principle of ion replacement based on the solubility difference as the driving force is an applicable strategy for fabricating various micro- and nanostructured oxides. The variation of pH values, reaction temperature, and $Mg_5(CO_3)_4(OH)_2$ reagent shapes can effectively vary the solubility of these two carbonate salts, which therefore tunes the final morphology of our obtained samples. Nevertheless, the preliminary findings here are expected to stimulate further investigation and development of the spontaneous replacement reaction, which may lead to new and important opportunities in the synthesis of many metal oxides and other low-dimensional materials by the spontaneous ion replacement reaction.

Supporting Information Available: Figures showing an IR spectrum and SEM images. This material is available free of charge via the Internet at http://pubs.acs.org.

Acknowledgment. The finical support from a Foundation for the Author of National Excellent Doctoral Dissertation of PR China (Grant No. 200322), the National Natural Science Foundation of China (Grant No. 20471012), and the Research Fund for the Doctoral Program of Higher Education (Grant No. 20040141004) is greatly acknowledged.

References and Notes

(1) Huang, Y.; Duan, X.; Cui, Y.; Lauhon, L.; Kim, K.; Lieber, C. M. *Science* **2001**, *294*, 1313.
(2) Morales, A. M.; Lieber, C. M. *Science* **1998**, *279*, 208.
(3) Bachtold, A.; Hadley, P.; Nakanishi, T.; Dekker, C. *Science* **2001**, *294*, 1317.
(4) Holms, J.; Johnston, K. P.; Doty, R. C.; Korgel, B. A. *Science* **2000**, *287*, 1471.
(5) Puntes, V. F.; Krishnan, K. M.; Alivisatos, A. P. *Science* **2001**, *291*, 2115.
(6) Sun, Y. G.; Xia, Y. N. *Science* **2002**, *298*, 2176.
(7) Kim, F.; Song, J. H.; Yang, P. D. *J. Am. Chem. Soc*. **2002**, *124*, 14316.
(8) (a) Zhu, Y.; Bando, Y.; Xue, D.; Golberg, D. *Adv. Mater*. **2004**, *16*, 831. (b) Zhu, Y.; Bando, Y.; Xue, D.; Golberg, D. *J. Am. Chem. Soc*. **2003**, *125*, 16196. (c) Xu, J.; Xue, D. *J. Phys. Chem. B* **2005**, *109*, 17157.
(9) Yan, C.; Xue, D. *J. Phys. Chem. B* **2005**, *109*, 12358.
(10) Gou, L. F.; Murphy, C. J. *Nano Lett*. **2003**, *3*, 231.

(11) Joo, J.; Kwon, S. G.; Yu, J. H.; Hyeon, T. *Adv. Mater*. **2005**, *17*, 1873.

(12) Alivisatos, A. P. *Science* **1996**, *271*, 933.

(13) Zarur, A. J.; Ying, J. Y. *Nature* **2000**, *403*, 65.

(14) Majetich, S. A.; Jin, Y. *Science* **1999**, *284*, 470.

(15) (a) Pan, Z. W.; Dai, Z. R.; Wang, Z. L. *Science* **2001**, *291*, 1947. (b) Tian, Z. R.; Voigt, J. A.; Liu, J., Mckenzie, B.; Mcdermott, M. J.; Rodriguez, M. A.; Konishi, H.; Xu, H. *Nature Mater*. **2003**, *2*, 821. (c) Huang, M. H.; Wu, Y.; Feick, H.; Tran, N.; Weber, E.; Yang, P. *Adv. Mater*. **2001**, *13*, 113. (d) Vayssieres, L. *Adv. Mater*. **2003**, *15*, 464.

(16) (a) Siegfried, M. J.; Choi, K. *Angew. Chem., Int. Ed*. **2005**, *44*, 3218. (b) Jiang, X.; Herricks, T.; Xia, Y. *Nano Lett*. **2002**, *2*, 1333. (c) Liu, B.; Zeng, H. C. *J. Am. Chem. Soc*. **2004**, *126*, 8124. (d) Yin, M.; Wu, C.; Lou, Y.; Burda, C.; Koberstein, J. T.; Zhu, Y.; Brien, S. O. *J. Am. Chem. Soc*. **2005**, *127*, 9506.

(17) Armstrong, A. R.; Bruce, P. G. *Nature* **1996**, *381*, 499.

(18) Seo, W. S.; Jo, H. H.; Lee, K.; Kim, B.; Oh, S. J.; Park, J. T. *Angew. Chem., Int. Ed*. **2004**, *43*, 1115.

(19) Liu, X.; Li, C.; Han, S.; Han, J.; Zhou, C. *Appl. Phys. Lett*. **2003**, *82*, 1950.

(20) Pang, Y., Bao, X. *J. Mater. Chem*. **2002**, *12*, 3699.

(21) Choi, K. S.; Lichtenegger, H. C.; Stucky, G. D. *J. Am. Chem. Soc*. **2002**, *124*, 12402.

(22) Liu, C. H.; Zapien, J. A.; Yao, Y.; Meng, X. M.; Lee, C. S.; Fan, S. S.; Lifshitz, Y.; Lee, S. T. *Adv. Mater*. **2003**, *15*, 838.

(23) Krumeich, F.; Muhr, H.-J.; Niederberger, M.; Bier, F.; Schnyder, B.; Nesper, R. *J. Am. Chem. Soc*. **1999**, *121*, 8324.

(24) Park, J.; Privman, V.; Matijevic, E. *J. Phys. Chem. B* **2001**, *105*, 11630.

(25) Boerlage, S.; Kennedy, M.; Witkamp, G.; Hoek, J.; Schippers, J. *J. Membrane Sci*. **1999**, *159*, 47.